Characterization of guided acoustic waves in an arbitrary direction with full-field instantaneous maps of the acoustic displacement

X. Luís Deán-Ben,[a] Cristina Trillo, Ángel F. Doval, and José L. Fernández
Departamento de Física Aplicada, Universidade de Vigo, E. T. S. Enxeñeiros Industriais, Campus Universitario, E36310 Vigo, Spain

(Received 1 May 2012; accepted 17 July 2012; published online 21 August 2012)

The full-field optical measurement of guided acoustic waves presents important advantages derived from the capability to map the acoustic field in a two dimensional region, so that acoustic information over a large area can be retrieved with each measurement. In this work, we introduce an extension of the well-established two dimensional spatio-temporal Fourier transform method to calculate the frequency spectrum of guided acoustic waves. For this, we take advantage of the unique capability of a self-developed double-pulsed television holography system to acquire the acoustic displacement field in two spatial dimensions and time. Then, the spatio-temporal Fourier transform method is expanded to three dimensions according to the nature of the experimental data, so that the frequency spectrum of the waves propagating in an arbitrary direction can be calculated. The method is tested experimentally by generating narrowband Lamb waves in an aluminium plate with a piezoelectric transducer. The good agreement between the theoretical and experimental spectra in a broad zone anticipates the applicability of the method to characterize guided acoustic waves as a function of the propagation direction in materials or structures presenting anisotropic propagation behaviour. © *2012 American Institute of Physics*. [http://dx.doi.org/10.1063/1.4745883]

I. INTRODUCTION

Guided acoustic waves are specific kinds of waves with applications in the inspection and characterization of materials and structures. Although compression and shear waves are the kind of ultrasonic waves most widely employed, guided acoustic waves present several important advantages to inspect and characterize beams, plate-like structures, rods, pipes, etc.[1] For example, the capability of these waves to propagate along large distances with low attenuation permits to perform the so-called long range inspection.[2]

Lamb waves are a well-known kind of guided acoustic waves that exist in plates with parallel and stress-free boundaries.[3] The applications of Lamb waves can generally be classified into two main groups, namely those leading to the detection and characterization of flaws and those leading to the dimensional and elastic characterization of the propagating medium. In particular, for the second purpose, experimental data of a given property of Lamb waves are obtained as a function of mode and frequency. This property can be the phase velocity,[4,5] the group velocity,[5,6] the wavelength,[7,8] or the wavenumber. In this last case, information of the frequency spectrum of the different propagating modes can be obtained in the form of discrete points, lines, or a bidimensional (2D) amplitude distribution in the frequency-wavenumber plane. The classical method to obtain a 2D distribution is based on the 2D Fourier transform (FT) of the spatio-temporal distribution of the stress or displacement caused by a Lamb wavetrain. It was first proposed by Alleyne and Cawley,[9] who used the classical wedge method to generate and to detect the wavetrains, recording the time history of the wave at equally spaced points.

Other authors have used the 2D FT method to characterize Lamb waves using different excitation and detection schemes. The aforementioned wedge method is reversible and can be employed both for the generation[10–15] and detection[15] of the waves. Other reversible methods were also used to acquire the experimental data, such as air-coupled transducers[16,17] and immersion transducers in a liquid-filled cell.[18,19] In all these methods, the detection is performed by sensing a compression wave generated, according to the Snell's law, by the guided wave. For a given inclination of the transducer, guided waves with the corresponding phase velocity are preferably detected, so that the transducer acts as a filter and the recorded waveform does not faithfully reproduce the actual guided wavetrain. A different method for acquiring the experimental data is laser ultrasonics. The laser generation of guided waves is usually performed by focusing the beam from a pulsed laser at the plate surface, so that broadband waves are generated, whereas the detection of guided wavetrains is usually performed by optical means, typically pointwise interferometers.[20–24]

The applicability of the 2D FT method is not limited to plates. In fact, several authors have reported the use of this method to calculate the frequency spectrum of guided waves in other structures, for example, cylinders[25,26] or wedge tips.[27] This method is also used to process data of the propagation of guided wavetrains simulated with numerical methods,[28–32] so that the theoretical frequency spectrum can be estimated in structures where the characteristic equation is complicated to solve. Other methods based on time-frequency transformations (e.g., short-time FT, wavelets, etc) can also be employed to estimate the frequency spectrum of broadband guided acoustic waves.[33]

In all the experimental set-ups described above, the acquisition procedure is the same as the one reported by

[a]Electronic mail: x.l.dean.ben@hotmail.com.

Alleyne and Cawley, i.e., a time-domain signal is recorded for a set of generation or detection points, which are selected with a scanning system. When using the discrete FT, the frequency range is determined by the sampling interval. The small spot size of focused laser beams allows to explore high spatial frequency zones of the spectrum if a short sampling interval is selected. This can be done both when scanning the generation[20–22] or the detection systems,[12,14] so that with this technology Lamb wavetrains with frequencies up to approximately 10 MHz were characterized.[20,21,27] Once selected the frequency range, i.e., the Nyquist frequency, then the frequency resolution is determined by the number of signal samples. For the temporal frequency, the resolution can be very fine since the number of samples of the time history at each point can be made very large. However, the resolution in the wavenumber is limited by the number of scanning steps, which is typically of the order of one hundred. In order to increase the resolution in the wavenumber, some authors pad with zeros in the space domain.[23,34] The implementation of a scanning system may be cumbersome, specially when using contact transducers that need to be coupled to the plate with a liquid layer. Furthermore, the fact of changing the excitation or detection points may lead to the lack of repeatability of the experiment. An array of transducers can be employed for acquiring the experimental data.[35] In this way, non-repeatability inconsistencies are avoided at the expense of a larger sampling interval.

On the other hand, full-field optical techniques allow to measure the acoustic displacement field in a two-dimensional region.[36–42] In this way, each full-field measurement covers a much larger area than a time-domain signal retrieved with a pointwise detection method, which is only affected by the propagation of the guided wave between the excitation and measuring points. Thereby, full-field optical techniques can potentially be used to characterize the propagation of guided acoustic waves in an arbitrary direction. In this work, we take advantage of the unique capability of a self-developed double-pulsed television holography (TVH) system to record the instantaneous acoustic displacement field caused by guided waves in plates. The displacement as a function of two spatial dimensions and time is measured by acquiring a sequence of maps under repeatability conditions corresponding to successive instants of the wave propagation. Then, we present an extension of the classical 2D FT method to calculate the frequency spectrum of the waves, which is based on the three-dimensional (3D) spatio-temporal FT of the experimental data. We have shown in a previous work that the application of the 3D FT significantly improves the signal-to-noise ratio (SNR) in the measurement of the wavenumber of quasi-monochromatic Lamb waves with respect to the 2D FT approach.[43] Herein, we analyse the capability of the 3D FT method to calculate a large region of the frequency spectrum of guided acoustic waves propagating in an arbitrary direction, an interesting feature for characterizing the waves in materials or structures presenting anisotropic propagation behaviour. The method is tested in two aluminium plates in which narrowband Lamb wavetrains are generated by means of a piezoelectric transducer pressed against the plate edge. Although in our case narrowband waves must be used to achieve a reasonable SNR, a broader zone of the spectrum can be measured without changing the piezoelectric position by recording sequences of maps corresponding to several wavetrains with different central frequencies, so that a wide zone of the spectrum is obtained by stitching the branches corresponding to each wavetrain. The agreement between the experimental frequency spectra and the theoretical ones is very good, which indicates the capability of the method to retrieve a large amount of information provided broadband acoustic waves with a reasonable SNR can be generated.

II. BACKGROUND

For the sake of completeness, we briefly review in this section the well-known characteristic equations of Lamb waves in isotropic media and the well-established implementation of the 2D FT method with the discrete FT. Thereby, the notation used in the following sections is also introduced.

A. Frequency spectrum of Lamb waves

For an isotropic and homogeneous plate, the relation between the circular frequency ω (or the frequency $f = \omega/2\pi$) and the wavenumber k_1 of a particular Lamb mode is established in the so-called Rayleigh-Lamb equation, which in adimensional form is given by

$$\frac{\tan\left[\frac{\pi}{2}\sqrt{\gamma^2\chi^2-\xi^2}\right]}{\tan\left[\frac{\pi}{2}\sqrt{\gamma^2-\xi^2}\right]}+\left[\frac{4\xi^2\sqrt{\gamma^2\chi^2-\xi^2}\sqrt{\gamma^2-\xi^2}}{\left(2\xi^2-\gamma^2\chi^2\right)^2}\right]^{\pm 1}=0. \tag{1}$$

The positive and negative exponents in Eq. (1) stand for the symmetric and antisymmetric modes, respectively. This classification of Lamb modes into two families is due to the type of symmetry of the displacement field with respect to the mean plane of the plate. The adimensional parameters of Eq. (1) are the normalized frequency $\gamma = 2h\omega/\pi c_L$, the normalized wavenumber $\xi = 2hk_1/\pi$, and the velocity ratio $\chi = c_L/c_T$, being $2h$ the plate thickness and c_L and c_T the phase velocities of the compression and shear waves in the plate material.

The solutions (k_1, ω) of Eq. (1) stand in a set of curves that correspond to the possible Lamb modes in the plate. The frequency spectrum of a band-limited wavetrain consists of a set of segments of the aforementioned curves inside the frequency band of the wavetrain. The frequency spectrum for real values of the wavenumber, namely the branches of the curves corresponding to the propagating modes, is represented in Fig. 1 for the first 10 symmetric and antisymmetric Lamb modes. These curves were calculated considering that $c_L = 6330\,\mathrm{m/s}$ and $c_T = 3117\,\mathrm{m/s}$, i.e., typical values of these wave velocities in aluminium.

B. The 2D spatio-temporal Fourier transform method

The experimental measurement of the frequency spectrum by means of the 2D spatio-temporal FT of the

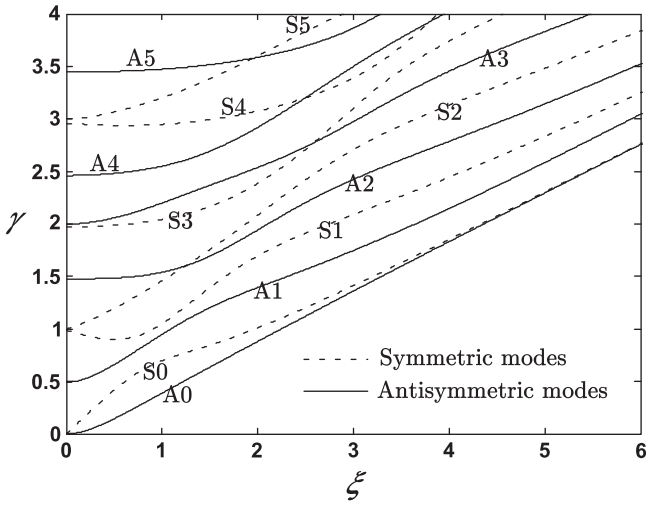

FIG. 1. Frequency spectrum for the first 10 propagating Lamb modes calculated considering $c_L = 6330\,\text{m/s}$ and $c_T = 3117\,\text{m/s}$.

experimental data was first proposed by Alleyne and Cawley[9] and, as stated in the introduction, many authors use this method to characterize guided acoustic waves. The starting point of the method is the experimental recording of a stress or displacement field at the plate surface for a set of N equally delayed instants and P equally spaced points along the propagating direction x_1. In order to explain the method, we consider that the experimental magnitude is the out-of-plane displacement field at the plate surface $u_3(x_1,t)$, being x_1 the direction of propagation of the wave and t the time. The experimental data can be expressed as

$$u_3(x_{1p},t_n) = u_3(x_{10}+p\Delta x_1, t_0+n\Delta t), \tag{2}$$

with $p = 0,\ldots,P-1$ and $n = 0,\ldots,N-1$. Δt and Δx_1 are the sampling intervals in time and along the actual plate coordinate x_1, respectively.

The method is based on the calculation of the 2D discrete FT of the experimental set of data, which is given by[44]

$$\tilde{u}_3(f_{p'},f_{n'}) = \frac{1}{\sqrt{PN}}\sum_{p=0}^{P-1}\sum_{n=0}^{N-1} u_3(x_{1p},t_n)\exp(2\pi i p p'/P) \times \exp(2\pi i n n'/N). \tag{3}$$

Then, the experimental frequency spectrum is obtained as a representation of the values of $\text{mod}[\tilde{u}_3(f_{p'},f_{n'})]$. The discrete spatial frequency along the direction of propagation $f_{p'}$ and the discrete temporal frequency $f_{n'}$ are given by

$$f_{p'} = \frac{p'}{P\Delta x_1} = \frac{k_1}{2\pi}, \tag{4}$$

$$f_{n'} = \frac{n'}{N\Delta t} = \frac{\omega}{2\pi}. \tag{5}$$

The value of $\tilde{u}_3(f_{p'},f_{n'})$ is calculated for a set of $P\times N$ points. p' and n' are integers given by

$$p' = -\frac{P}{2},\ldots,\frac{P}{2}, \tag{6}$$

$$n' = -\frac{N}{2},\ldots,\frac{N}{2}, \tag{7}$$

where the two extreme values of p' and n' correspond Nyquist or critical frequency range. The values of $\tilde{u}_3(f_{p'},f_{n'})$ for these extreme values are not independent (in fact they are equal), but all others are. The resolution of the frequency spectrum, i.e., the difference between two consecutive temporal and spatial frequencies is given by

$$\Delta f_{p'} = \frac{1}{P\Delta x_1}, \tag{8}$$

$$\Delta f_{n'} = \frac{1}{N\Delta t}. \tag{9}$$

III. MATERIALS AND METHODS

A. Measurement of the acoustic displacement field

Our group has developed in the last decade a double-pulsed TVH system with the capability to measure guided acoustic waves in plates with amplitudes of a few nanometers. TV holography, also termed electronic speckle pattern interferometry, is a full-field interferometric technique based on the electronic recording of correlograms, which are formed by superimposing a reference beam to the object beam backscattered by the part to be measured.[45] In our case, the variable part of the object optical phase difference $\phi_o(\mathbf{x},t)$, i.e., the component of the optical phase depending on the change in the position of the object points, is proportional to the instantaneous out-of-plane displacement field $u_3(\mathbf{x},t)$ at the plate surface as follows[46]

$$\phi_o(\mathbf{x},t) = -\frac{4\pi}{\lambda}u_3(\mathbf{x},t), \tag{10}$$

where λ is the wavelength of the illumination laser and $\mathbf{x} = (x_1,x_2)$ is the position at the plate surface.

In our system, pulsed illumination is used. Each correlogram encodes the information of the surface displacement field at the instant in which the surface is illuminated as the duration of the pulse is much smaller than the period of the acoustic wave. Two correlograms are recorded corresponding to two laser pulses delayed a short time, and a processing procedure based on the spatial FT method (SFTM)[47] is applied in order to obtain the optical phase-change $\Delta\Phi(\mathbf{x},t_r,t)$ between the recording instants, which is related to $\phi_o(\mathbf{x},t)$ as

$$\Delta\Phi(\mathbf{x},t_r,t) = \phi_o(\mathbf{x},t) - \phi_o(\mathbf{x},t_r), \tag{11}$$

where t_r and t are the instants of emission of the first and second laser pulses, respectively.

Two synchronization set-ups can be employed. In the first one, which we call the static-reference set-up, the first pulse is emitted with the plate at rest and the second one with the wavetrain in the field of view. Taking into account Eqs. (10) and (11), the optical phase-change is given by

$$\Delta\Phi(t,\mathbf{x}) = -\frac{4\pi}{\lambda}u_3(t,\mathbf{x}). \tag{12}$$

The second set-up, which we call the dynamic-reference set-up, consists in emitting both pulses with the wavetrain in the field of view and an interval between pulses of n_T half-periods of the acoustic wave, where n_T is an odd number. This set-up is more appropriate for measuring quasi-monochromatic waves, in which the acoustic frequency f_0 is well-defined. Again taking into account Eqs. (10) and (11), the optical phase-change is given by

$$\Delta\Phi(\mathbf{x},t) = -\frac{4\pi}{\lambda}\left[u_3(\mathbf{x},t) - u_3\left(\mathbf{x}, t - \frac{n_T}{2f_0}\right)\right]. \tag{13}$$

For narrowband wavetrains, the maps obtained with the static-reference set-up faithfully represent the instantaneous shape of the plate surface, whereas the resulting SNR is higher with the dynamic-reference set-up. For a set of maps obtained with increasing t and for a given point $\mathbf{x}_0$, the temporal FT of $\Delta\Phi(\mathbf{x}_0,t)$ is given by

$$\Delta\tilde{\Phi}(\mathbf{x}_0,f) = -\frac{4\pi}{\lambda}\tilde{u}_3(\mathbf{x}_0,f), \tag{14}$$

$$\Delta\tilde{\Phi}(\mathbf{x}_0,f) = -\frac{4\pi}{\lambda}[1 - \exp(-\mathrm{i}\pi n_T f/f_0)]\tilde{u}_3(\mathbf{x}_0,f), \tag{15}$$

where Eqs. (14) and (15) correspond to the static-reference and the dynamic-reference set-ups, respectively. $\tilde{u}_3(\mathbf{x}_0,f)$ is the temporal Fourier transform of $u_3(\mathrm{x}_0,t)$. In the case that the wavetrain has a relatively broad bandwidth, f_0 is taken as its central acoustic frequency. Therefore, the shape of $\Delta\tilde{\Phi}(\mathbf{x}_0,f)$ differs from the shape of $\tilde{u}_3(\mathbf{x}_0,f)$ in a factor $[1 - \exp(-\mathrm{i}\pi n_T f/f_0)]$ when using the dynamic-reference set-up. However, the modulus of this factor is higher than 1 when

$$\frac{f_0}{3n_T} < f < \frac{5f_0}{3n_T}. \tag{16}$$

Therefore, for a bandwidth lower than $4f_0/3n_T$, although the shape of $\Delta\tilde{\Phi}(\mathbf{x}_0,f)$ calculated with the dynamic-reference set-up is not equal to the shape of $\tilde{u}_3(\mathbf{x}_0,f)$, its modulus is higher than the corresponding $\Delta\tilde{\Phi}(\mathbf{x}_0,f)$ calculated with the static-reference set-up. Taking into account that the detection system works in near saturation, shot-noise limited regime,[48] the average noise level in each correlogram is the same in both set-ups and a higher SNR in the spectrum is obtained with the dynamic-reference set-up. The constant $4f_0/3n_T$ is higher with low values of n_T so that it is preferable to use the lowest possible odd number.

B. The 3D spatio-temporal Fourier transform method

The excitation pulser of our system is synchronized with the laser pulses in such a way that the delay between the beginning of the excitation burst and the instant of emission of the pulses can be accurately controlled. Then, if the acquisition is repeated with a different delay between excitation and detection, a map corresponding to the same wavetrain at a different instant is obtained, provided repeatability conditions apply.

The hypothesis of repeatability conditions is fulfilled in our case as we do not change the excitation or detection systems during the whole experiment.

Therefore, a set of 2D maps corresponding to successive instants t of the wavetrain propagation are obtained (see Eqs. (12) and (13)), so that the experimental data consist of a 3D array of the optical phase-change $\Delta\Phi$ as a function of two spatial dimensions (x_1,x_2) and time t, which is proportional to the instantaneous out-of-plane displacement field, i.e., the actual set of experimental data can be expressed as

$$u_3(x_{1p},x_{2q},t_n) = u_3(x_{10}+p\Delta x_1, x_{20}+q\Delta x_2, t_0+n\Delta t), \tag{17}$$

with $p = 0,\ldots,P-1$, $q = 0,\ldots,Q-1$, and $n = 0,\ldots,N-1$. Δt, Δx_1, and Δx_2 are the sampling intervals in time and space along the horizontal and vertical directions, respectively.

Then, the 3D FT of this set of data is given by[44]

$$\begin{aligned}\tilde{u}_3(f_{p'},f_{q'},f_{n'}) = \frac{1}{\sqrt{PQN}}\sum_{p=0}^{P-1}\sum_{q=0}^{Q-1}\sum_{n=0}^{N-1}u_3(x_{1p},x_{2q},t_n)\\ \times\exp(2\pi\mathrm{i}pp'/P)\exp(2\pi\mathrm{i}qq'/Q)\\ \times\exp(2\pi\mathrm{i}nn'/N).\end{aligned} \tag{18}$$

The values of $f_{p'}$ and $f_{n'}$ are given by Eqs. (4) and (5), respectively, whilst the value of the vertical spatial frequency $f_{q'}$ is given by

$$f_{q'} = \frac{q'}{Q\Delta x_2}. \tag{19}$$

The value of $\tilde{u}_3(f_{p'},f_{q'},f_{n'})$ is calculated for $P\times Q\times N$ points, where p' and n' are integers given by Eqs. (6) and (7), respectively, whereas q' is given by

$$q' = -\frac{Q}{2},\ldots,\frac{Q}{2}. \tag{20}$$

Then, the resolution in the vertical spatial frequency is given by

$$\Delta f_{q'} = \frac{1}{Q\Delta x_2}. \tag{21}$$

Usually, the modulus of the projection of the 3D FT in the plane $(f_{p'},f_{q'})$ has only significative values inside a region like that represented in Fig. 2. The angle α represents the main direction of propagation of the wavetrain and β is related to the divergence of the beam (which produces

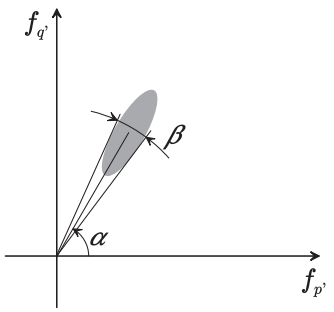

FIG. 2. Modulus of the projection of $\tilde{u}_3(f_{p'},f_{q'},f_{n'})$ in the plane $(f_{p'},f_{q'})$.

geometric attenuation). For a quasi-plane wavetrain, the angle β is small and a 2D spatio-temporal spectrum is enough to describe the wave, taking the spatial frequencies f_α in the direction corresponding to the angle α.

For simplicity, considering wavetrains propagating along the horizontal direction x_1, the frequency spectrum is calculated as the modulus of $\tilde{u}_3(f_{p'},0,f_{n'})$, where

$$\tilde{u}_3(f_{p'},0,f_{n'}) = \frac{1}{\sqrt{Q}}\sum_{q=0}^{Q-1}\frac{1}{\sqrt{PN}}\sum_{p=0}^{P-1}\sum_{n=0}^{N-1}u_3(x_{1p},x_{2q},t_n) \times \exp(2\pi i p p'/P)\exp(2\pi i n n'/N). \quad (22)$$

The 2D spectrum given by Eq. (22) is proportional to the average, calculated for all the horizontal rows of the map, of the 2D FT of Eq. (3), so that the SNR is improved with respect to a single 2D spectrum of a horizontal row.

If the wavetrain is not plane, the 3D FT contains information of the frequency spectrum of Lamb waves propagating in the directions contained in $\alpha \pm \beta/2$. In particular, for a cylindrical wave (excited for example with a point source on the plate surface) the angle β is 360°, so we can obtain information about the frequency spectrum in an arbitrary direction. If the plate is isotropic, as in our case, the frequency spectrum is the same regardless of the propagation direction.

The propagation of a narrowband wavetrain can be described in terms of the phase and group velocities, c_p and c_g, respectively,[5] in a way that the time T_{FW} required for the propagation of the wavetrain along the whole field of view is of the order of

$$T_{FW} = \frac{D_F + D_W}{c_g}, \quad (23)$$

where D_F is the size of the field of view in the propagation direction and D_W the wavetrain length. No additional information is obtained if the acquisition time exceeds T_{FW}, as the wavetrain would propagate outside the field of view. Also, once selected the acquisition time $T_S = (N-1)\Delta t$, no additional information is obtained for a field of view larger than

$$D_{FW} = T_S c_g + D_W, \quad (24)$$

as the wavetrain would not reach at any time a region of the field of view. Therefore, the size of the field of view and the number N of optical phase-change maps must be selected jointly.

In the case that higher resolution in the spectrum is needed, a solution consists in padding with zeros both in space and time, so that the spatial and temporal size of data are increased. However, we must take into account that the SNR is reduced. In our experiments, we did not consider this option.

The 3D FT of the experimental set of data was calculated by means of an implementation of the Cooley-Tukey fast Fourier transform (FFT) algorithm,[44] which requires that the input data are integer powers of two.

In the experiments, we considered the largest possible field of view achievable with our current system set-up. The size of the field of view was $224 \times 56\,\text{mm}^2$ (which corresponds to $1024 \times 256\,\text{pixel}^2$). The sampling interval was $\Delta x_1 = 224/1024\,\text{mm}$, which is much smaller than half the minimum wavelength, i.e., faraway from the Nyquist limit in space. In each experiment, a set of $N = 256$ maps was acquired corresponding to successive instants of propagation delayed a quantity Δt small enough to satisfy the Nyquist criterion in time.

C. Bandwidth of the wavetrains

The number of cycles of the excitation burst is related to the spectral density amplitude and to the bandwidth of the corresponding frequency spectrum. As a matter of fact, when the number of pulses is higher, the SNR in the frequency spectrum increases but a narrower bandwidth is obtained.

In our experimental system, a narrowband source must be used in order to reach a SNR high enough to give useful information of the frequency spectrum. A key point to select the number of cycles to be used in the experiments is to establish a trade-off between the bandwidth and the SNR of the resulting spectrum. In spite of the former limitation, a broader zone of the frequency spectrum can be obtained without any changes in the measuring hardware by stitching the spectra recorded in different experiments using narrowband wavetrains with different central frequencies. These two issues are experimentally realized and discussed in the present work.

D. Test plates

The experiments were performed in two aluminium plates with nominal thicknesses 1 and 4 mm (alloy denominations EN AW 6082-T6 and EN AW 2017A-T4, respectively). The transversal dimensions of the plates are $500 \times 200\,\text{mm}^2$, so that the wavetrains can travel a relatively large distance (and the measurements are completed) before being reflected at the plate edges.

The thickness and phase velocities of the compression and shear waves in the materials of the plates were measured in two previous works, resulting $2h = 0.987\,\text{mm}$, $c_L = 6283\,\text{m/s}$, and $c_T = 3116\,\text{m/s}$ for the first plate[43] and $2h = 4.013\,\text{mm}$, $c_L = 6371\,\text{m/s}$, and $c_T = 3107\,\text{m/s}$ for the second plate.[8]

The plates were supported so that the constraints at their surface were negligible; they simply rested on a horizontal board covered in velvet fabric.

E. Description of the experimental system

The Lamb wavetrains were excited by means of a piezoelectric transducer and detected with our double-pulsed TVH system. The layout of the experimental system is depicted in Fig. 3.

A piezoelectric transducer with a central frequency of 1 MHz was used to excite narrowband multimode Lamb waves in the aluminium plates. As shown in Fig. 3, it was directly coupled to an edge of the plate. Then, the waves were generated by exciting the piezoelectric with a tone-burst consisting of a few cycles with a given central frequency.

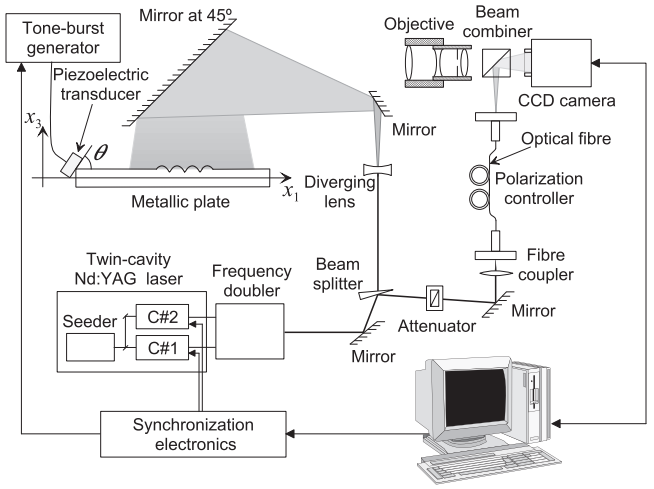

FIG. 3. Layout of the experimental system.

The Lamb wavetrains were measured with a self-developed double-pulsed TVH system as described in Sec. III A, yielding the instantaneous out-of-plane acoustic displacement field at the plate surface. The core of the system is a frequency-doubled twin-cavity seeded Q-switched Nd:YAG laser, which was used as the illumination source to produce two correlograms that were recorded in separate frames of a CCD camera (PCO SensiCam Double Shutter).

As described in Sec. III A, two possible synchronizations set-ups can be used, yielding two respective optical phase-change maps given by Eqs. (12) and (13). In the range of frequencies employed, the number of half-periods between laser pulses used was $n_T = 3$, limited by the minimum delay between exposures of the camera.

IV. RESULTS

A. Frequency spectrum corresponding to a single individual wavetrain

A first experiment was performed in order to compare the branches of the frequency spectrum obtained with the two possible synchronization set-ups and with different number of cycles of the excitation burst. A set of wavetrains with a central frequency of 1.000 MHz were generated in the plate 0.987 mm thick. The excitation bursts that we used in these experiments consisted of 2, 3, 4, 5, 6, 8, and 10 cycles, respectively. The temporal sampling interval, i.e., the delay between two successive maps was $\Delta t = 250$ ns. Each frequency spectrum is calculated by means of the 3D spatio-temporal FT method (Eq. (22)).

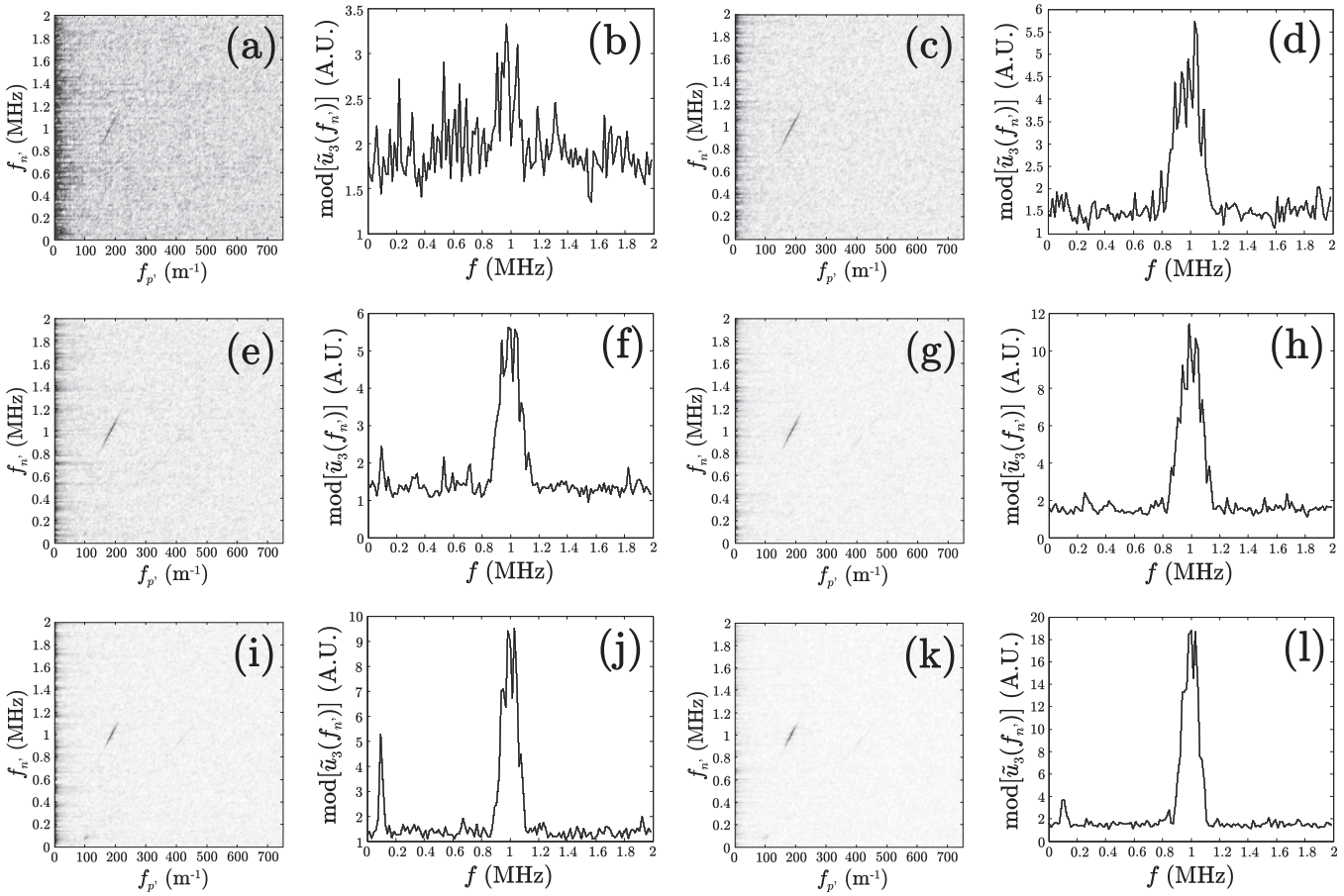

FIG. 4. Frequency spectra obtained with the static-reference and dynamic-reference set-ups for wavetrains with a central frequency of 1.000 MHz in the aluminium plate 0.987 mm thick. The first and third columns show the modulus of $\tilde{u}_3(f_{p\prime}, 0, f_{n\prime})$ (Eq. (22)) for the static-reference and dynamic-reference set-ups, respectively, being $f_{p\prime}$ and $f_{n\prime}$ given by Eqs. (4) and (5). The second and fourth columns display the maximum amplitude projection of the first and third columns, respectively, in the frequency axis (neglecting the 20 lowest values of the spatial frequency). The wavetrains consist of 3 cycles (first row), 5 cycles (second row), and 8 cycles (third row).

TABLE I. Bandwidth and SNR of the frequency spectra corresponding to the wavetrains employed in the experiment described in Sec. IV A for the static-reference and dynamic reference set-ups.

	Static reference		Dynamic reference	
Number of cycles	Bandwidth (kHz)	SNR	Bandwidth (kHz)	SNR
2	…	…	…	…
3	…	…	245	14.6
4	212	17.3	217	17.1
5	208	18.4	196	20.2
6	166	16.1	145	23.3
8	132	18.3	131	29.9
10	122	20.3	122	33.2

The first and third columns of Fig. 4 show the frequency spectra obtained for the wavetrains consisting of 3, 5, and 8 cycles corresponding to the static-reference and dynamic-reference set-ups, respectively. The respective maximum amplitude projections of the amplitude spectral density in the frequency axis are shown in the second and fourth columns of Fig. 4. Such projections are calculated neglecting the 20 lowest values of the spatial frequency (where the noise is too high). No significant difference in the shape of the amplitude spectral density is detected when calculating the spectrum with any of the two synchronization set-ups.

The bandwidth of the wavetrains is estimated as the full width at half maximum (FWHM) in the second and fourth columns of Fig. 4 and is displayed in Table I.

We define the SNR as the ratio between the mean value of the signal and the root mean square of the noise, i.e.,

$$\mathrm{SNR} = \frac{\{\mathrm{mod}[\tilde{u}_{3,\mathrm{signal}}(f_{p'}, 0, f_{n'})]\}_{\mathrm{mean}}}{\{\mathrm{mod}[\tilde{u}_{3,\mathrm{noise}}(f_{p'}, 0, f_{n'})]\}_{\mathrm{rms}}}. \quad (25)$$

A point in the spectra of Fig. 4 is considered signal when the amplitude spectral density is higher than 6 times the standard deviation of the noise in the region of interest (the 20 lowest values of the spatial frequency were neglected to perform the calculation due to the high level of noise in this region). The rest of the points of the region of interest are considered noise (we assume white noise). The value of the SNR obtained thereby is shown in Table I for the static-reference and dynamic-reference set-ups, respectively. As expected, the SNR increases with the number of pulses of the excitation burst and it is also higher in the dynamic reference set-up than in the static reference set-up.

B. Frequency spectrum corresponding to a set of wavetrains

In a second experiment, a broader zone of the frequency spectrum is obtained by stitching the spectra calculated as described in Sec. III B (Eq. (22)) with different wavetrains having different central frequencies. The stitching corresponds to the sum of the moduli of $\tilde{u}_3(f_{p'}, 0, f_{n'})$ (Eq. (22)) corresponding to each frequency, being $f_{p'}$ and $f_{n'}$ given by Eqs. (4) and (5), respectively. The dynamic-reference set-up was used to record wavetrains of 5 cycles in the two plates described in Sec. III D.

A good repeatability is obtained because no changes are made in the optomechanical hardware between recordings, only the central frequency of the piezoelectric driver output is changed. This central frequency can be selected from a set of values given by $20/(A+1)$ MHz, being A an integer between 31 and 13, i.e., the frequencies range from 0.625 MHz to 1.429 MHz. The delay between two consecutive maps was set in all cases to $\Delta t = 200$ ns.

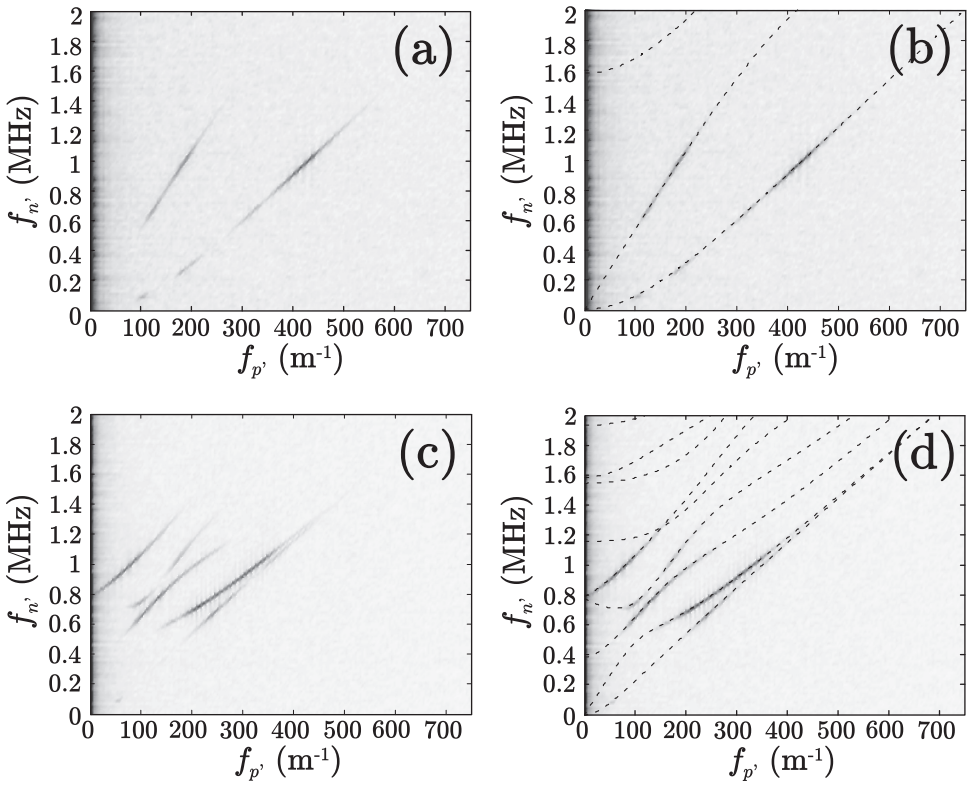

FIG. 5. Experimental frequency spectra obtained by stitching the resulting frequency spectra corresponding to a set of narrowband wavetrains with different central frequencies. (a) and (b) Plate 0.987 mm thick. (c) and (d) Plate 4.013 mm thick. The experimental frequency spectra are shown in (a) and (c) and the experimental frequency spectra superimposed to the theoretical ones calculated from the plate parameters stated in Sec. III D are displayed in (b) and (d).

The result of the experiment is shown in Fig. 5, where the theoretical curves for the parameters of the plates stated in Sec. III D are also displayed. As shown in the second column of Fig. 5, the agreement between the experimental frequency spectrum and the theoretical curves is very good.

It is worth commenting that in the frequency spectra of Fig. 4 only a branch corresponding to the S0 Lamb mode is yielded, while in the frequency spectrum shown in the first row of Fig. 5 (which corresponds to the same plate) both the A0 and the S0 Lamb modes are detected. The experiments described in Secs. IV A and IV B were made in different conditions. The angle θ shown in Fig. 3 was smaller in the experiment described in Sec. IV B, which benefits the generation of the A0 Lamb mode.

V. DISCUSSION AND CONCLUSIONS

A novel approach to a well-established method based on the two dimensional spatio-temporal Fourier transform to calculate the frequency spectrum of guided acoustic waves was introduced. While in the classical approach a set of single-point time-domain signals are recorded, in the present paper the experimental data were obtained from a sequence of maps of the instantaneous displacement field corresponding to successive instants of the propagation of the wavetrain. For this, we took advantage of the unique capability of a self-developed double-pulsed TV holography system to render a two dimensional map of the instantaneous out-of-plane displacement field at the surface of a plate. From the acquired experimental data, we proposed a method to calculate the frequency spectrum based on the three dimensional spatio-temporal Fourier transform. The method was analysed theoretically, and we established its potential applicability to calculate the frequency spectrum as a function of the propagating direction.

The proposed method was tested in two aluminium plates in which we generated narroband Lamb wavetrains by means of a piezoelectric transducer. We analysed the results obtained with the two possible synchronization set-ups of our TV holography system and we established that the so-called dynamic-reference set-up is more appropriate to perform the measurements. In our case, a broad zone of the frequency spectrum was calculated by stitching the branches of the frequency spectrum obtained with several wavetrains at different frequencies, since repeatability conditions apply because the experimental hardware is not changed or moved during the experiments. The agreement between the experimental frequency spectra and the theoretical curves was very good in the whole frequency range for the two plates used in the experiments. Then, the method can potentially be applied to calculate a broad zone of the frequency spectrum of guided acoustic waves in an arbitrary direction.

In conclusion, the application of the 3D Fourier transform to the data acquired with double-pulsed TV holography allows accurately determining a broad zone of the frequency spectrum of guided acoustic waves. The capability of the method to calculate the frequency spectrum in an arbitrary direction may have important applications in the characterization of anisotropic plates or other structures presenting anisotropic propagation behaviour. The generation of broadband acoustic waves with an amplitude large enough to guarantee an acceptable signal-to-noise ratio, which may be achieved by laser excitation, remains, however, a challenge to be addressed.

ACKNOWLEDGMENTS

This work was co-funded by the University of Vigo (Contract No. 09VIA07), the Spanish Ministerio de Ciencia e Innovación, and the European Commission (ERDF) in the context of the Plan Nacional de I+D+i (Project No. DPI2008-02709). Financial support from the Dirección Xeral de Investigación, Desenvolvemento e Innovación da Xunta de Galicia in the context of the Plan Galego de IDIT (Project No. INCITE08PXIB303252PR) is also acknowledged.

[1]D. E. Chimenti, "Guided waves in plates and their use in materials characterization," Appl. Mech. Rev. **50**(5), 247–284 (1997).
[2]P. Cawley and D. Alleyne, "The use of Lamb waves for the long range inspection of large structures," Ultrasonics **34**(2-5), 287–290 (1996).
[3]I. A. Viktorov, *Rayleigh and Lamb Waves* (Plenum, New York, 1967).
[4]W. P. Rogers, "Elastic property measurement using Rayleigh-Lamb waves," Res. Nondestruct. Eval. **6**(4),185–208 (1995).
[5]X. L. Deán-Ben, C. Trillo, A. F. Doval, and J. L. Fernández, "Phase and group velocities measurement of ultrasonic guided wavetrains in plates by pulsed TV holography," J. Acoust. Soc. Am. **127**(4), 2210–2219 (2010).
[6]Y. Hayashi, S. Ogawa, H. Cho, and M. Takemoto, "Non-contact estimation of thickness and elastic properties of metallic foils by the wavelet transform of laser-generated Lamb waves," NDT & E Int. **32**(1), 21–27 (1999).
[7]J. L. Fernández, J. L. Deán, C. Trillo, and A. F. Doval, "Elastic constants determination by direct measurement of the beat wavelength between A0 and S0 Lamb modes with pulsed TV holography," Opt. Lasers Eng. **45**(5), 618–630 (2007).
[8]J. L. Deán, C. Trillo, A. F. Doval, and J. L. Fernández, "Determination of thickness and elastic constants of aluminum plates from full-field wavelength measurements of single-mode narrowband Lamb waves," J. Acoust. Soc. Am. **124**(3), 1477–1489 (2008).
[9]D. Alleyne and P. Cawley, "A two-dimensional Fourier transform method for the measurement of propagating multimode signals," J. Acoust. Soc. Am. **89**(3), 1159–1168 (1991).
[10]T. Hayashi and K. Kawashima, "Single mode extraction from multiple modes of Lamb wave and its application to defect detection," JSME Int. J. **46**(4), 620–626 (2003).
[11]I. Nuñez, R. K. Ing, C. Negreira, and M. Fink, "Transfer and Green functions based on modal analysis for Lamb waves generation," J. Acoust. Soc. Am. **107**(5), 2370–2378 (2000).
[12]B. Morvan, N. Wilkie-Chancellier, H. Duflo, A. Tinel, and J. Duclos, "Lamb wave reflection at the free edge of a plate," J. Acoust. Soc. Am. **113**(3), 1417–1425 (2003).
[13]D. Leduc, B. Morvan, P. Pareige, and J.-L. Izbicki, "Measurement of the effects of rough surfaces on Lamb waves propagation," NDT & E Int. **37**(3), 207–211 (2004).
[14]N. Wilkie-Chancellier, L. Martinez, S. Serfaty, P. Griesmar, E. Caplain, J.-Y. Le Huerou, and M. Gindre, "Lamb mode reflections at the end of a plate loaded by a viscoelastic material," Ultrasonics **44**(Suppl. 1), e863–e868 (2006).
[15]D.-A. Ta, Z.-Q. Liu, and X. Liu, "Combined spectral estimator for phase velocities of multimode Lamb waves in multilayer plates," Ultrasonics **44**(Suppl. 1), e1145–e1150 (2006).
[16]M. Cinquin, M. Castaings, B. Hosten, P. Brassier, and P. Pérès, "Monitoring of the moisture content in carbon-epoxy plates using Lamb waves," NDT & E Int. **38**(1), 37–44 (2005).
[17]M. Castaings and B. Hosten, "Ultrasonic guided waves for health monitoring of high-pressure composite tanks," NDT & E Int. **41**(8), 648–655 (2008).
[18]R. Balasubramanyam, D. Quinney, R. E. Challis, and C. P. D. Todd, "A finite-difference simulation of ultrasonic Lamb waves in metal sheets with experimental verification," J. Phys. D **29**(1), 147–155 (1996).

[19]C. P. D. Todd and R. E. Challis, "Quantitative classification of adhesive bondline dimensions using Lamb waves and artificial neural networks," IEEE Trans. Ultrason. Ferroelectr. Freq. Control **46**(1), 167–181 (1999).
[20]C. Eisenhardt, L. J. Jacobs, and J. Qu, "Application of laser ultrasonics to develop dispersion curves for elastic plates," J. Appl. Mech. **66**(4), 1043–1045 (1999).
[21]W. Gao, C. Glorieux, and J. Thoen, "Laser ultrasonic study of Lamb waves: determination of the thickness and velocities of a thin plate," Int. J. Eng. Sci. **41**(2), 219–228 (2003).
[22]Y. Shi, S.-C. Wooh, and M. Orwat, "Laser-ultrasonic generation of Lamb waves in the reaction force range," Ultrasonics **41**(8), 623–633 (2003).
[23]S. G. Pierce, B. Culshaw, W. R. Philp, F. Lecuyer, and R. Farlow, "Broadband Lamb wave measurements in aluminium and carbon/glass fibre reinforced composite materials using non-contacting laser generation and detection," Ultrasonics **35**(2), 105–114 (1997).
[24]X. Zhang, T. Jackson, and E. Lafond, "Noncontact determination of elastic moduli by two-dimensional Fourier transformation and laser ultrasonic technique," Rev. Sci. Instrum. **76**(2), 026113 (2005).
[25]M. Kley, C. Valle, L. J. Jacobs, J. Qu, and J. Jarzynski, "Development of dispersion curves for two-layered cylinders using laser ultrasonics," J. Acoust. Soc. Am. **106**(2), 582–588 (1999).
[26]L. Martinez, B. Morvan, and J. L. Izbicki, "Space-time-wave number-frequency $Z(x,t,k,f)$ analysis of SAW generation on fluid filled cylindrical shells," Ultrasonics **42**(1-9), 383–389 (2004).
[27]S.-W. Tang and C.-H. Yang, "Dispersion behaviors of antisymmetric flexural modes propagating along wedge tips with a layer of thin coating," Jpn. J. Appl. Phys. Part 1 **46**(9), 5935–5938. (2007).
[28]F. Moser, L. J. Jacobs, and J. Qu, "Modeling elastic wave propagation in waveguides with the finite element method," NDT & E Int. **32**(4), 225–234 (1999).
[29]Y. L. Koh, W. K. Chiu, and N. Rajic, "Integrity assessment of composite repair patch using propagating Lamb waves," Compos. Struct. **58**(3), 363–371 (2002).
[30]L. Laguerre, A. Grimault, and M. Deschamps, "Ultrasonic transient bounded-beam propagation in a solid cylinder waveguide embedded in a solid medium," J. Acoust. Soc. Am. **121**(4), 1924–1934 (2007).
[31]J. Koreck, C. Valle, J. Qu, and L. J. Jacobs, "Computational characterization of adhesive layer properties using guided waves in bonded plates," J. Nondestruct. Eval. **26**(2–4), 97–105 (2007).
[32]B. Hosten and M. Castaings, "FE modeling of Lamb mode diffraction by defects in anisotropic viscoelastic plates," NDT & E Int. **39**(3), 195–204 (2006).
[33]M. Niethammer, L. J. Jacobs, J. Qu, and J. Jarzynski, "Time-frequency representations of Lamb waves," J. Acoust. Soc. Am. **109**(5), 1841–1847 (2001).
[34]S. Grondel, C. Paget, C. Delebarre, J. Assaad, and K. Levin, "Design of optimal configuration for generating A0 Lamb mode in a composite plate using piezoceramic transducers," J. Acoust. Soc. Am. **112**(1), 84–90 (2002).
[35]F. El Youbi, S. Grondel, and J. Assaad, "Signal processing for damage detection using two different array transducers," Ultrasonics **42**(1-9), 803–806 (2004).
[36]T. D. Mast and G. A. Gordon, "Quantitative flaw reconstruction from ultrasonic surface wavefields measured by electronic speckle pattern interferometry," IEEE Trans. Ultrason. Ferroelectr. Freq. Control **48**(2), 432–444 (2001).
[37]K. L. Telschow, V. A. Deason, D. L. Cottle, and J. D. Larson, "Full-field imaging of gigahertz film bulk acoustic resonator motion," IEEE Trans. Ultrason. Ferroelectr. Freq. Control **50**(10), 1279–1285 (2003).
[38]G. Pedrini, W. Osten, and M. E. Gusev, "High-speed digital holographic interferometry for vibration measurement," Appl. Opt. **45**(15), 3456–3462 (2006).
[39]J. L. Fernández, A. F. Doval, C. Trillo, J. L. Deán, and J. C. López, "Video ultrasonics by pulsed TV holography: A new capability for non-destructive testing of shell structures," Int. J. Optomechatron. **1**(2), 122–153 (2007).
[40]S. Li, K. D. Mohan, W. W. Sanders, and A. L. Oldenburg, "Toward soft-tissue elastography using digital holography to monitor surface acoustic waves," J. Biomed. Opt. **16**(11), 116005 (2011).
[41]C. Trillo, A. F. Doval, F. Mendoza-Santoyo, C. Pérez-López, M. de la Torre-Ibarra, and J. L. Deán, "Multimode vibration analysis with high-speed TV holography and a spatiotemporal 3D Fourier transform method," Opt. Express **17**(20), 18014–18025 (2009).
[42]S. Muñoz Solís, F. Mendoza Santoyo, and M. S. Hernández-Montes, "3d displacement measurements of the tympanic membrane with digital holographic interferometry," Opt. Express **20**(5), 5613–5621 (2012).
[43]X. L. Deán-Ben, C. Trillo, A. F. Doval, and J. L. Fernández, "Fast characterization of aluminum plates with TV-holography measurements of the frequency spectrum of multimode, quasi-monochromatic Lamb waves," IEEE Trans. Ultrason. Ferroelectr. Freq. Control **58**(6), 1222–1231 (2011).
[44]W. H. Press, B. P. Flannery, S. A. Teukolsky, and W. T. Vetterling, *Numerical Recipes in C* (Cambridge University Press, Cambridge, 1988), pp. 407–414.
[45]A. F. Doval, "A systematic approach to TV holography," Meas. Sci. Technol. **11**(1), R1–R36 (2000).
[46]C. Trillo, D. Cernadas, A. F. Doval, C. López, B. V. Dorrío, and J. L. Fernández, "Detection of transient surface acoustic waves of nanometric amplitude with double-pulsed TV holography," Appl. Opt. **42**(7), 1228–1235 (2003).
[47]C. Trillo, A. F. Doval, D. Cernadas, O. López, J. C. López, B. V. Dorrío, J. L. Fernández, and M. Pérez-Amor, "Measurement of the complex amplitude of transient surface acoustic waves using double-pulsed TV holography and a two-stage spatial Fourier transform method," Meas. Sci. Technol. **14**(12), 2127–2134 (2003).
[48]D. Cernadas, C. Trillo, A. F. Doval, J. C. Lopez, B. V. Dorrio, J. L. Fernandez, and M. Perez-Amor, "Non-destructive testing with surface acoustic waves using double-pulsed tv holography," Meas. Sci. Technol. **13**(4), 438–444 (2002).